Molecular-beam epitaxy growth of low-threshold cw GaInNAsSb lasers at 1.5 μm

Seth R. Bank,[a] Mark A. Wistey, Homan B. Yuen, Lynford L. Goddard, Hopil Bae, and James S. Harris, Jr.
Solid State and Photonics Laboratory, Stanford University, Stanford, California 94305

(Received 27 October 2004; accepted 21 March 2005; published 13 June 2005)

The solid-source molecular-beam epitaxial growth of low-threshold GaAs-based GaInNAsSb lasers is discussed. A general narrowing of the growth window was observed with increasing wavelength, due to the increased nitrogen required ($\geqslant$1%), and has historically made high-performance devices more difficult to achieve beyond $\sim$1.35 μm. The introduction of antimony and reduction in plasma-related damage from the rf nitrogen source dramatically improved material quality and widened the growth window. We validate these observations with 1.5 μm edge-emitting ridge-waveguide lasers with cw threshold current densities as low as 440 A/cm^2, peak CW output powers of 431 mW, peak cw wallplug efficiencies $>$16%, and pulsed output powers $>$1 W.
 [DOI: 10.1116/1.1914825]

I. INTRODUCTION

The demonstration of band gap narrowing in InGaAs with the introduction of nitrogen by Kondow and co-workers has prompted intense research towards high-performance GaAs-based lasers at 1.3 and 1.55 μm.[1–7] The inherently high gain of GaInNAs and GaInNAsSb quantum wells (QWs), $>$1500 cm^{-1} per QW,[3,4,6] and the achievable output powers make these materials quite promising for high-power applications, including Raman amplification and solid-state laser pumping. Nitrogen affects primarily the conduction band, which results in both large conduction band offsets and electron effective mass, significantly reducing electron leakage.[1] Consequently, the characteristic temperatures of the threshold current density T_0, and the external efficiency T_1, are typically higher than for InP-based devices. For vertical-cavity surface-emitting lasers, the availability of the lattice-matched Al(Ga)As/GaAs layers allows for high-reflectivity distributed mirrors with excellent thermal conductivity. Moreover, native oxide layers for current and optical confinement provide further performance enhancement.

GaInNAs is a metastable alloy and has proven to be significantly more difficult to grow than InP-based materials. Low growth temperature causes significant defect densities that require postgrowth annealing. For molecular-beam epitaxy (MBE)-grown material, ion damage[8] and contamination from the rf plasma cell used to generate reactive nitrogen are important issues. Metalorganic chemical vapor deposition (MOCVD) suffers from hydrogen contamination that significantly degrades lifetime by forming N-H complexes and gallium vacancies.[9] Despite these difficulties, both MBE and MOCVD-grown 1.3 μm GaInNAs lasers have shown superior threshold current density, output power, and characteristic temperatures to their InP counterparts.[3,4] The typical design methodology is to introduce only the minimum amount of nitrogen needed to achieve the desired operating wavelength. For 1.3 μm, the nitrogen content can be held to $<$1% and laser performance is only slightly degraded compared to 1.2 μm InGaAs lasers.

Higher nitrogen content, on the order of 2.5%–4%, are required for the 1.5 μm regime, and growth becomes significantly more challenging.[5–7] A reduction of QW growth temperature is necessary and all growth and postgrowth parameters must be re-optimized, including group III growth rates, nitrogen gas flow, arsenic overpressure, and annealing temperature. The addition of antimony relaxes the growth requirements somewhat by promoting smooth two-dimensional growth and reducing the amount of nitrogen required.[10] Despite the addition of antimony, a strong increase in threshold current with wavelength had hitherto been observed in all dilute-nitride lasers beyond $\sim$1.3 μm. This was dubbed the "nitrogen penalty" and appeared to be an unavoidable degradation mechanism. Recent results, however, indicate that this is not an insurmountable obstacle.[6,7]

Herein, we describe the growth and fabrication of low-threshold lasers in the 1.5 μm regime with performance comparable to many of the best reports $\sim$1.3 μm. Important considerations that are discussed include wavelength control, nitrogen plasma cell operation, annealing condition optimization, and arsenic capping. Deflection plate voltage optimization,[8] plasma stability,[11] and arsenic capping[12] are also discussed elsewhere in greater detail.

II. MBE GROWTH

Group III metals were supplied by SUMO effusion cells, arsenic by a conventional valved cracker, antimony by an unvalved cracker, and nitrogen by a rf plasma cell. Dopants were supplied by silicon (*n*-type) and carbon tetrabromide (*p*-type). Growth rates were measured by beam-equivalent pressure (BEP), calibrated to x-ray diffraction (InGaAs) and white-light reflectivity (AlGaAs/GaAs). Typical growth rates, substrate temperatures, and arsenic overpressures for Ga(N)As, GaInNAsSb, and (Al)GaAs are given in Table I.

[a]Electronic mail: sbank@stanfordalumni.org

TABLE I. Typical growth parameters for materials used in laser and PL growths at ~1.5 μm. Approximate growth temperature windows for the dilute-nitride materials, over which the peak PL intensity remains >50% of optimal, are given in parentheses.

Material	Growth rate (μm/h)	Growth temperature (approximate range)	Arsenic overpressure (times group III flux)
GaAs before QW	0.28–0.3	440 °C	3–4×
GaNAs	0.28–0.3	440 °C (400–550 °C)	15×
GaInNAsSb	0.45–0.5	440 °C (420–460 °C)	20×
AlGaAs	1.0	600 °C	15×

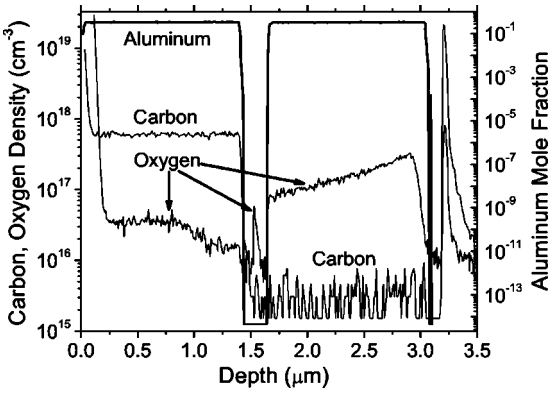

FIG. 1. SIMS measurement of carbon, oxygen, and aluminum in a 1.3 μm laser structure. Both carbon and oxygen are seen to increase in the QW (depth ~1.5 μm).

Nitrogen incorporation was controlled directly by the group III growth rate g_r (μm/h): $N\% = C/g_r$.[13] The constant $C \approx 0.8$ for Ga(In)NAs, but increases somewhat in the presence of antimony.[14] The SVT Associates cell was operated under fairly standard conditions: 300 W input power and 0.5 sccm gas flow. Purity of the nitrogen gas has been found to be essential for growth of high quality material. To this end, we employed 99.999% purity nitrogen gas, followed by a <1 part-per-billion purifier (Pall Mini-Gaskleen), and minimized the backstreaming of impurities during the vent-run and run-vent transitions. Oxygen and water peaks were below the sensitivity limit of $\sim 2 \times 10^{-13}$ Torr of the residual gas analyzer with 0.25 sccm of input nitrogen gas. Figure 1 shows secondary-ion mass spectrometry (SIMS) measurements of residual oxygen, nitrogen, and carbon levels throughout a 1.3 μm laser structure. From integration of the SIMS peaks, contamination levels in the QW were found to be: carbon 3×10^{16} cm^{-3}, oxygen 3×10^{17} cm^{-3}, and hydrogen (not shown) 2.5×10^{18} cm^{-3}. Aluminum content was the same in the QW and the GaAs waveguide region, $\sim 10^{8}$ cm^{-3}.

To maximize run-to-run stability, the plasma was "prelit" prior to the first growth of the day and run to stabilization. The plasma was extinguished and the chamber was allowed to return to ultra-high vacuum before sample introduction. To minimize ion-related damage, biased deflection plates were employed at the exit aperture. Samples were grown at the bias (−40 V and ground) that produced the minimum total current from remote Langmuir probe measurements.[8] More recent work indicates this is nonoptimal, and somewhat higher deflection voltages may likely show added improvement.

Arsenic capping was also employed to protect the wafer surface during the plasma ignition, capacitively to inductively coupled transition, and stabilization. After growth of the GaAs buffer layer and/or bottom waveguide, growth was paused and the wafer was cooled for approximately an hour, to a minimum of ~40 °C, under an arsenic flux of BEP $\sim 1.5 \times 10^{-6}$ Torr. The reflection high-energy electron diffraction (RHEED) pattern changed during the cooling process, from a 2×4 reconstructed GaAs surface to several concentric semicircles, indicating polycrystalline arsenic deposition, and finally to that of amorphous arsenic. The plasma was then ignited and run to stabilization with the MBE shutter closed. The wafer was subsequently heated to growth temperature, desorbing the cap. From RHEED, we estimate a 30–45 s gap (~75–100 °C) between arsenic decapping and arrival at the QW growth temperature, at which point growth was reinitiated. The RHEED pattern was seen to degrade during this time, possibly due to contamination from the nitrogen gas source or plasma exposure. We may rule out contamination, however, using SIMS. While it is difficult to tell from Fig. 1, as the resolution is degraded at the depths of the QW (~1.5 μm), SIMS measurements of similar but shallower QW structures showed no increase in carbon, oxygen, hydrogen, or boron at the arsenic capping/decapping interface. Nitrogen buildup to a mole fraction of ~1% was observed in the SIMS profile, however. This nitrogen incorporation and/or concurrent plasma-related damage may cause a portion of the remaining nonradiative recombination observed in the lasers presented here.

Photoluminescence (PL) samples and ridge-waveguide lasers were grown on (100) GaAs wafers. The active layer for all samples discussed here was a single 75 Å $Ga_{0.62}In_{0.38}N_{0.023}As_{0.95}Sb_{0.027}$ quantum well surrounded on either side by 220 Å $GaN_{0.025}As_{0.975}$ barriers, both grown at ~440 °C. The antimony BEP was $\sim 1.2 \times 10^{-7}$ Torr. For PL experiments, the active layer was grown on a 3000 Å GaAs buffer and capped with 500 Å of GaAs. Samples were cleaved into pieces and *ex situ* annealed over a range of temperatures 700–820 °C for one minute in a rapid thermal annealing furnace. Arsenic out diffusion was minimized by a proximity cap. Lasers were embedded in a $GaAs/Al_{0.33}Ga_{0.67}As$ waveguide and both deflection plates and arsenic capping were employed. A more detailed description of the laser structure and fabrication is given elsewhere.[6] Pieces of the laser material were annealed at several temperatures, but the results presented here are for a postgrowth anneal performed at 740 °C for 1 min.

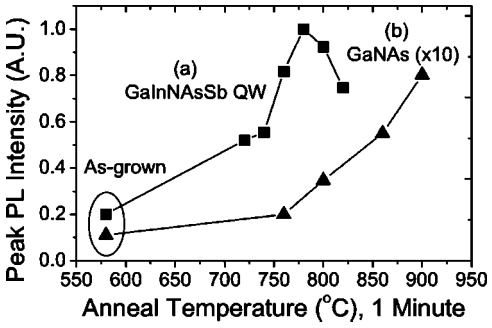

FIG. 2. Peak PL intensity as a function of annealing temperature for (a) a GaInNAsSb QW surrounded by GaAs barriers and (b) a GaNAs layer surrounded by GaAs barriers. The product of the two is qualitatively the same as that of a GaInNAsSb QW surrounded by GaNAs barriers.

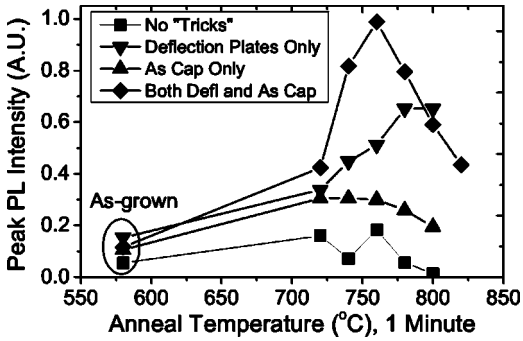

FIG. 3. A comparison of peak PL intensity as a function of annealing temperature, for several GaInNAsSb/GaNAs QW samples grown with different plasma damage reduction techniques.

III. PHOTOLUMINESCENCE

PL is an excellent tool for examining the optical quality of dilute-nitride materials due to its extremely high sensitivity to point defects. Many samples appear to be of excellent quality in high-resolution x-ray diffraction (HR-XRD) and transmission electron microscopy (TEM), but show poor or degraded optical quality in PL. This is a crucial point for dilute-nitride optimization as it is point defects that appear to limit high-performance devices: structurally, the material appears nearly flawless. Moreover, higher PL efficiency has been observed in some samples with clearly inferior HR-XRD and TEM quality. PL efficiency appears to be the best method for gauging optical quality and predicting laser performance.[4]

To optimize laser performance, it is important to optimize the postgrowth annealing of the *entire* active region. Figure 2 illustrates this point with the annealing behavior of a GaInNAsSb QW sample, surrounded by GaAs barriers, and another sample containing a GaNAs layer surrounded by GaAs. The GaInNAsSb QW shows maximal PL efficiency at a much lower temperature than the GaNAs layer. It is important to optimize the anneal to balance the competing effects. It is noted that the product of the two curves reproduce the annealing behavior of a GaInNAsSb QW surrounded by GaNAs barriers, to within a constant scaling factor. Barrier material quality is an important consideration due to the importance of carrier leakage in these devices.

Similarly, growth techniques strongly affect the annealing behavior. The peak PL intensity with annealing temperature is plotted in Fig. 3 for several different samples grown with and without arsenic capping, and with and without deflection plates. In general, we have observed that the rollover of peak PL with annealing temperature generally occurs at higher temperatures for samples with higher PL efficiency. The primary exception is the case of arsenic capping, which improves PL intensity but reduces the rollover temperature. The likely conclusion is that the cap removes some damage due to ignition and stabilization, but other defects are added by surface nitridation between the arsenic cap desorption and the initiation of growth. The result is an overall improvement in PL efficiency and a reduction in optimal anneal temperature.

IV. WAVELENGTH CONTROL

With a five-element system, wavelength control and repeatability become important practical considerations. Group III sources are quite straightforward to control with BEP measurements. The nitrogen content, which depends directly on the growth rate, is also well controlled—if the cell is always run to stabilization under the same conditions (gas flow, cell temperature, and rf forward and reflected power). Arsenic overpressure does not appear to significantly affect emission wavelength, however, only 15× and 20× BEP have been attempted at the long wavelengths. The emission wavelength is also a weak function of the antimony flux. By doubling the antimony flux, from 1×10^{-7} Torr flux to 2×10^{-7} Torr, the peak emission was redshifted by ~10 meV, indicating that 5% flux control is required for 1 nm wavelength control. This emission difference persisted over the entire range of anneal temperatures studied.

The emission wavelength is, however, a strong function of the substrate temperature. Nominally identical samples grown at progressively higher temperatures, as measured with both band-edge spectroscopy and pyrometry, showed a linear blueshift of 1.5 meV per 20 °C of increasing temperature, as grown. The difference increased to 5.6 meV/20 °C under optimal annealing conditions, due to the increasing optimal anneal temperature. This indicates ±0.92 °C control is required for 1 nm precision of the annealed emission wavelength and underscores the need for substantially more accurate temperature control than oxide blowoff temperature or thermocouple. The blueshift in emission with increasing substrate temperature is contrary to the observations of the Infineon group for GaInNAs.[7] For the as-grown samples, this is likely due to the incorporation kinetics of antimony. Due to the low growth temperature, the antimony desorption rate is likely minimal and a large surface concentration already exists. As a result, reducing the substrate temperature to "freeze" the antimony into the alloy is more successful than simply increasing the flux. The result is a more highly strained QW emitting at a longer wavelength, consistent with

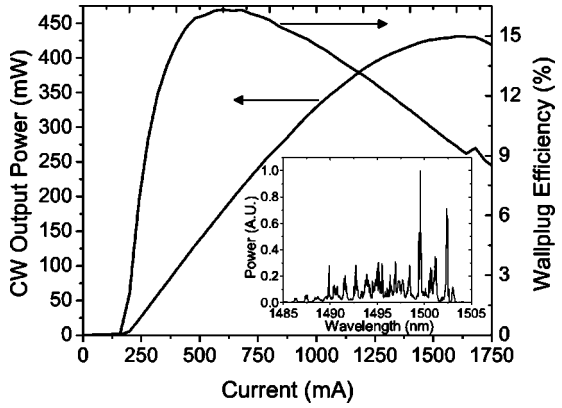

FIG. 4. 15 °C CW *L-I* and wallplug efficiency curves for a 20 μm $\times$2150 μm laser. Inset shows optical spectrum at maximum output power.

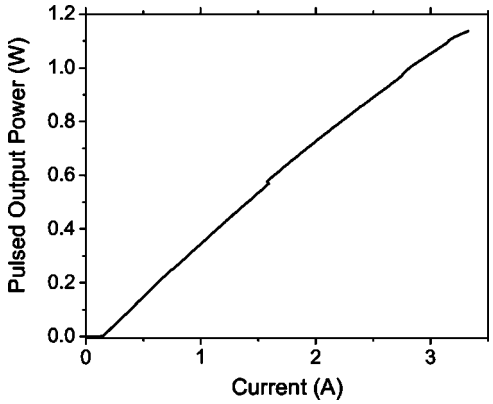

FIG. 5. Pulsed room temperature *L-I* curve a 20 μm $\times$ 1220 μm device.

the HR-XRD and PL measurements. For annealed material that would be used in practical applications, differences in the optimal annealing temperature dominate the emission wavelength. Further study is needed to examine the root cause(s) of this behavior.

V. LASER RESULTS

Figure 4 shows the CW *L-I* curve and wallplug efficiency for a 20 μm $\times$ 2150 μm device mounted epi-side up with as-cleaved facets, at an ambient temperature of 15 °C (active region ~25 °C). The threshold current density was 440 A/cm^2, the external efficiency was 51%, and the peak output power was 431 mW from both facets. A peak wallplug efficiency of 16.3% was measured at 180 mW of output power. As shown in the inset of Fig. 4, the device lased at 1.50 μm at thermal rollover. Cw lasing was observed up to 65 °C, at a junction temperature of 90–95 °C. Under pulsed operation (500 ns pulse, 0.1% duty cycle), a 20 μm $\times$1220 μm laser produced substantially higher output powers at room temperature, as shown in Fig. 5. The threshold current density was 450 A/cm^2, the external efficiency was 49%, and a driver-limited peak output power of 1.145 W was achieved from both facets. The characteristic temperatures for the threshold current density T_0 and the external efficiency T_1 were 73 and 125 K, respectively. These are lower than previously reported 1.5 μm devices (106 and 208 K) due to a reduction in the temperature insensitive nonradiative component of the threshold current.

VI. CONCLUSION

Many of the MBE growth techniques required to produce high-quality dilute-nitride layers emitting in the 1.5 μm range have been outlined. Addition of antimony, reduction in plasma related damage, improvement of nitrogen gas purity, and reduced growth temperatures were keys to recent improvements in the 1.5 μm range. With improved MBE growth, the threshold current density has been progressively reduced. Low-threshold, high-efficiency, 1.5 μm edge-emitting lasers have been demonstrated to validate these improved growth techniques. Further optimization is required as the wavelength is extended due to increased nitrogen. In passing, we note that comparable optical quality has also been obtained at 1.55 μm with optimization, and it is likely the "nitrogen penalty" is more of a "nitrogen complexity"—separate growth optimization is required at each desired wavelength (i.e., each nitrogen concentration).

ACKNOWLEDGMENT

The authors acknowledge A. Moto of Sumitomo Electric Industries Ltd. for useful discussions, S. Zou of Santur for assistance with wafer thinning, Charles Evans and Associates for SIMS measurements, and Luxtron for the use of the pyrometer. This work was supported under DARPA contracts DAAD17-02-C-0101 and MDA972-00-1-0024, MARCO Interconnect Focus Center Contract MDA972-99-1-0002 and the Stanford Network Research Center (SNRC).

[1]M. Kondow, T. Kitatani, S. Nakatsuka, M. C. Larson, K. Nakahara, Y. Yazawa, M. Okai, and K. Uomi, IEEE J. Sel. Top. Quantum Electron. **3**, 719 (1997).
[2]M. C. Larson, C. W. Coldren, S. G. Spruytte, H. E. Petersen, and J. S. Harris Jr., 58th Dev. Rec. Conf., 2000.
[3]N. Tansu, J. Y. Yeh, and L. J. Mawst, IEEE J. Sel. Top. Quantum Electron. **9**, 1220 (2003).
[4]D. A. Livshits, A. Yu Egorov, and H. Riechert, Electron. Lett. **36**, 1382 (2000).
[5]L. H. Li, V. Sallet, G. Patriarche, L. Largeau, S. Bouchoule, L. Travers, and J. C. Harmand, Appl. Phys. Lett. **83**, 1298 (2003).
[6]S. R. Bank, M. A. Wistey, L. L. Goddard, H. B. Yuen, V. Lordi, and J. S. Harris Jr., IEEE J. Quantum Electron. **40**, 656 (2004).
[7]G. Jaschke, R. Averbeck, L. Geelhaar, and H. Riechert, J. Cryst. Growth **278**, 224 (2005).
[8]J. S. Harris, S. R. Bank, M. A. Wistey, and H. B. Yuen, IEE Proc.-Commun. **151**, 407 (2004).
[9]A. J. Ptak, S. Kurtz, M. H. Weber, and K. G. Lynn, J. Cryst. Growth **22**, 1584 (2004).
[10]V. Gambin, W. Ha, M. A. Wistey, H. Yuen, S. R. Bank, S. M. Kim, and J. S. Harris Jr., IEEE J. Sel. Top. Quantum Electron. **8**, 795 (2002).
[11]M. A. Wistey, S. R. Bank, H. B. Yuen, and J. S. Harris Jr., J. Cryst. Growth **278**, 229 (2005).
[12]M. A. Wistey, S. R. Bank, H. B. Yuen, and J. S. Harris Jr., J. Vac. Sci. Technol. B (these proceedings).
[13]S. G. Spruytte, M. C. Larson, W. Wampler, C. W. Coldren, H. E. Petersen, and J. S. Harris Jr., J. Cryst. Growth **227–228**, 506 (2001).
[14]K. Volz, V. Gambin, W. Ha, M. A. Wistey, H. Yuen, S. Bank, and J. S. Harris, J. Cryst. Growth **251**, 360 (2003).